INTERNATIONAL JOURNAL FOR NUMERICAL METHODS IN FLUIDS
Int. J. Numer. Meth. Fluids 2004; **45**:157–178 (DOI: 10.1002/fld.649)

An accurate moving grid Eulerian Lagrangian localized adjoint method for solving the one-dimensional variable-coefficient ADE

Anis Younes*,†

Laboratoire de Génie industriel, Université de la Réunion, 15 avenue René Cassin, BP 7151-97715 St Denis Cedex 09, La Réunion, France

SUMMARY

An accurate finite-volume Eulerian Lagrangian localized adjoint method (ELLAM) is presented for solving the one-dimensional variable coefficients advection dispersion equation that governs transport of solute in porous medium. The method uses a moving grid to define the solution and test functions. Consequently, the need for spatial interpolation, or equivalently numerical integration, which is a major issue in conventional ELLAM formulations, is avoided.

After reviewing the one-dimensional method of ELLAM, we present our strategy and detailed calculations for both saturated and unsaturated porous medium. Numerical results for a constant-coefficient problem and a variable-coefficient problem are very close to analytical and fine-grid solutions, respectively. The strength of the developed method is shown for a large range of CFL and grid Peclet numbers.

KEY WORDS: advection dispersion equation; Eulerian methods; Lagrangian methods; moving grid

1. INTRODUCTION

Advection dispersion equations (ADE) can be encountered in many physics domains such as fluid dynamics, atmospheric modelling, petroleum reservoir simulation, transport of solutes in groundwater, transport of chemical contaminants through the unsaturated zone of the porous medium, etc.

The numerical solution of the ADE, which we also call the transport equation, can be obtained with Eulerian methods, Lagrangian methods, or Characteristic methods.

With Eulerian methods, the equation is solved on a fixed spatial frame. Classical Eulerian methods are finite element (FE) and finite difference (FD) methods. For the

*Correspondence to: A. Younes, Laboratoire de Génie industriel, Université de la Réunion, 15 avenue René Cassin, BP 7151-97715 St Denis Cedex 09, La Réunion, France.
†E-mail: anis.younes@univ-reunion.fr

Received 27 December 2002
Revised 14 July 2003

convective dominated transport, these methods often generate numerical solutions with artificial diffusion and/or non-physical oscillations. Special schemes have been developed to solve the transport equation with FD or FE. Upwind methods, which have been introduced in FD [1], give first-order accurate stable schemes (with no oscillations) but with too much numerical diffusion smearing the front. To overcome this problem, high-order accurate and non-oscillatory FD upwind schemes have been developed [2, 3]. These schemes are generally constructed through a discontinuous piecewise polynomial representation of the solution [2] and are stabilized with slope limiters.

Numerical problems associated with Eulerian approaches are mainly due to the first-order advection term in the transport equation. Eulerian methods carry out the temporal discretization in the time direction, so they cannot accurately simulate all of the wave interactions that take place if the information propagates more than one cell per time step (i.e. if the CFL condition is violated), either for the reason of stability (for explicit methods) or for the reason of accuracy (for implicit methods) [4]. The CFL constraint can be very restrictive when the domain presents non-uniform spatial discretization. Another drawback of Eulerian methods is that the numerical solution is often dependent on grid orientation [5].

Lagrangian methods, such as the random walk method, employ a moving co-ordinate system to obtain solutions. The mass transport in porous media may be described by a macroscopic driving force, (advection) to which some random fluctuations are added. The random fluctuations are due to the velocity variations around the average velocity in correlation with permeability variations of the porous matrix observed at a macroscopic scale. However, these methods rapidly become very expensive and one must be very careful when the code is used in heterogeneous media [6]. Moreover, few references could be found in the literature on the application of these methods to multidimensional advective–diffusive–reactive transport equations.

Another class of methods, are characteristic methods. They use a Lagrangian treatment of the advective part by tracking particles along the characteristics and Eulerian treatment on the fixed grid of the dispersive part of the transport equation. Because the solutions of transport PDEs are much smoother along the characteristics than they are in the time direction, characteristic methods generate accurate solutions even if large time steps are used [7]. Characteristic methods have been widely investigated in numerical simulations of ADE in porous media (References [8–12], among others).

The Eulerian–Lagrangian localized adjoint method (ELLAM) is an improved characteristic method introduced first by Celia *et al.* [13]. ELLAM uses space-time test functions. It has the same performance as characteristic methods, guaranties mass conservation and treats general boundary conditions naturally in its formulation.

Different ELLAM schemes for the one dimensional ADE based on different (forward or backward) techniques for the tracking of characteristics are investigated [14, 15]. Finite-volume ELLAM where the test space has lower continuity than the solution space has been developed in References [16–18].

Celia and Zisman [19] and Ewing and Wang [15, 20, 21] generalized ELLAM schemes for one-dimensional advection–diffusion–reaction transport equation. ELLAM was also extended to two dimensions in References [22–26] and was used to simulate the solute transport in the unsaturated zone by Binning [24] and Binning and Celia [25].

In the literature ELLAM results remain however open to criticism since they can present numerical dispersion and/or oscillations. Indeed, conventional ELLAM formulations use a

fixed grid, defining the solution and the test functions relative to that fixed grid at every time step. In general, the fictitious particle (the food of characteristic lines) does not coincide with the fixed Eulerian nodes and interpolation must be used to obtain the Lagrangian values. The accuracy of Lagrangian-Eulerian approaches depends on the order of interpolation. While a high order interpolation could greatly reduce numerical dispersion, it can reintroduce spurious oscillation depending on the problem [7, 17].

On the other hand, many have come to recognize mesh adaptation as an effective tool for simulating sharp fronts and reducing numerical dispersion and oscillations (see for example References [27, 28]).

Therefore, the aim of this work is to combine ELLAM and mesh adaptation. We develop a new finite-volume Eulerian Lagrangian localized adjoint method using a moving spatial grid to define the solution and test functions of ELLAM. The need for spatial interpolation, or equivalently numerical integration, which is a major issue in conventional ELLAM formulations, is avoided.

Numerical experiments, given in the last part of the paper, show the accuracy and efficiency of the new method for both constant-coefficient and variable-coefficient problems and for a large range of CFL and grid Peclet numbers.

2. THE EULERIAN–LAGRANGIAN LOCALIZED ADJOINT METHOD (ELLAM)

2.1. Introduction

In this work, we are interested in the numerical solution of the following one dimensional ADE:

$$L(C) = \frac{\partial(\theta(x,t)C(x,t))}{\partial t} + \frac{\partial(q(x,t)C(x,t))}{\partial x} - \frac{\partial}{\partial x}\left(D(x,t)\frac{\partial C(x,t)}{\partial x}\right) = 0 \tag{1}$$

This equation governs the transport of a conservative constituent with concentration $C(x,t)$ in a porous medium, which can be partially or completely saturated with water [29].

The mass balance equation for the fluid, without sink/source terms, in the unsaturated region [29] is

$$\frac{\partial(\theta(x,t))}{\partial t} + \frac{\partial(q(x,t))}{\partial x} = 0 \tag{2}$$

where $q(x,t)$ is the Darcy's velocity (LT^{-1}) and $\theta(x,t)$ the volumetric water content.

We use the standard formulation of the dispersion coefficient with $D(x,t) = \lambda_L|q| + \theta D_m\tau$. $|q|$ is the magnitude of the Darcy's velocity, λ_L is the longitudinal pore-scale dispersivity (L) which may be a non-linear function of the saturation [30–33]. D_m is the molecular diffusion coefficient in free water (L^2T^{-1}) and τ is the tortuosity factor, assumed to be a given function of the water content θ and the saturation water content θ_S.

$L(C)$ is the differential operator defined by (1). The equation is defined in the domain Ω_{xt}, and is subject to initial and boundary conditions:

$$C(x,0) = C_0(x)$$

$$C(x,t) = g_1(x,t) \qquad (x \in \partial\Omega_x^1, t > 0)$$

$$\left(-D\,\frac{\partial C(x,t)}{\partial x}\right).n_{\partial\Omega} = g_2(x,t) \qquad (x \in \partial\Omega_x^2, t > 0)$$

$$\left(qC(x,t) - D\,\frac{\partial C(x,t)}{\partial x}\right).n_{\partial\Omega} = g_3(x,t) \quad (x \in \partial\Omega_x^3, t > 0)$$

$\partial\Omega_x^1$ corresponds to the Dirichlet boundary condition, $\partial\Omega_x^2$ corresponds to the Neumann boundary condition and $\partial\Omega_x^3$ corresponds to the total flux boundary condition.

In theory the three kinds of boundary condition can be applied at the inflow or the outflow boundary. However, in practice in groundwater solute transport problems, we use almost exclusively a Dirichlet boundary condition or a total flux boundary condition at the inflow. For the outflow boundary, the Neumann condition with no dispersive flux is used almost exclusively. Therefore, only these configurations will be detailed in this work.

One notices that when solving (1), on the spatial domain Ω for the unknown $C(x,t)$ and for $t \in [0,T]$, Darcy's velocity $q(x,t)$ and water content $\theta(x,t)$ are assumed to be known and they verify the fluid mass balance equation (2).

The spatial domain $\Omega = [0,l]$ is partitioned into nm intervals or finite volumes $\Omega_i^0 = [x_{i-1/2}^0, x_{i+1/2}^0]$ of distance Δx_i, where x_i^0 is the centre of the interval and $x_{i+1/2}^0$ defined by

$$x_{i+1/2}^0 = \begin{cases} x_{1/2}^0 = 0 \\ \dfrac{x_i^0 + x_{i+1}^0}{2} \qquad (0 < i < nm) \\ x_{nm+1/2}^0 = l \end{cases} \tag{3}$$

Time is divided into discrete and not necessarily equal intervals $\Delta t^{n+1} = t^{n+1} - t^n$.

2.2. Variational formulation

The weak formulation of Equation (1), using space-time test functions $\omega = \omega(x,t)$ gives:

$$\int_0^T \int_\Omega L(C)\omega = \int_0^T \int_\Omega \left[\frac{\partial(\theta C)}{\partial t}\,\omega + \frac{\partial(qC)}{\partial x}\,\omega - \frac{\partial}{\partial x}\left(D\,\frac{\partial C}{\partial x}\right)\omega\right] \mathrm{d}x\,\mathrm{d}t = 0 \tag{4}$$

$\omega(x,t)$ vanish for $t \notin [t^{n+1}, t^n]$.

Using the following relationships:

$$\frac{\partial(\theta C)}{\partial t}\,\omega = \frac{\partial(\omega\theta C)}{\partial t} - C\theta\,\frac{\partial\omega}{\partial t} \tag{5}$$

$$\frac{\partial(qC)}{\partial x}\,\omega = \frac{\partial(qC\omega)}{\partial x} - qC\,\frac{\partial\omega}{\partial x} \tag{6}$$

$$\frac{\partial}{\partial x}\left(D\frac{\partial C}{\partial x}\right)\omega = \frac{\partial}{\partial x}\left(\omega D\frac{\partial C}{\partial x}\right) - D\frac{\partial C}{\partial x}\frac{\partial \omega}{\partial x} \tag{7}$$

we obtain from (4),

$$\int_0^T\int_\Omega \left[\frac{\partial(\theta\omega C)}{\partial t} - C\left(\theta\frac{\partial\omega}{\partial t} + q\frac{\partial\omega}{\partial x}\right) + \frac{\partial}{\partial x}\left(\left(qC - D\frac{\partial C}{\partial x}\right)\omega\right) + D\frac{\partial C}{\partial x}\frac{\partial\omega}{\partial x}\right]\mathrm{d}x\,\mathrm{d}t = 0 \tag{8}$$

$\theta(\partial\omega/\partial t) + q(\partial\omega/\partial x)$ is the adjoint associated to the hyperbolic part of L.

Since $\omega = \omega(x,t)$, the material derivative of ω is defined by

$$\frac{\mathrm{d}\omega}{\mathrm{d}t} = \frac{\partial\omega}{\partial t} + \frac{\mathrm{d}x}{\mathrm{d}t}\frac{\partial\omega}{\partial x} = \frac{\partial\omega}{\partial t} + V(x,t)\frac{\partial\omega}{\partial x} \tag{9}$$

where $V(x,t)$ is the fluid velocity related to the Darcy velocity by

$$V(x,t) = q(x,t)/\theta(x,t) \tag{10}$$

ELLAM method selects $\omega(x,t)$ so as to make the adjoint integral of $\theta(\partial\omega/\partial t) + q(\partial\omega/\partial x)$ vanish for all x and t. $\omega(x,t)$ must therefore be constant along the characteristics. Moreover, to conserve mass, the test function should sum to 1 [13].

With this choice of ω, the ADE (8) to solve becomes

$$\int_0^T\int_\Omega \left[\frac{\partial(\theta\omega C)}{\partial t} + \frac{\partial}{\partial x}\left(\omega\left(qC - D\frac{\partial C}{\partial x}\right)\right) + D\frac{\partial C}{\partial x}\frac{\partial\omega}{\partial x}\right]\mathrm{d}x\,\mathrm{d}t = 0 \tag{11}$$

2.3. Tracking

Let $x(t) = X(t;\tilde{x},\tilde{t})$ be the characteristic passing through a given point $(\tilde{x},\tilde{t})$, with $\tilde{t}\in[t^n, t^{n+1}]$, and determined by the following system of equations

$$\begin{cases} \mathrm{d}x(t)/\mathrm{d}t = V(x(t),t) \\ x(\tilde{t}) = \tilde{x} \end{cases} \tag{12}$$

This notation can refer to tracking forward or backward in time; in particular, we define

$$\begin{aligned} x^* &= X(t^n; x, t^{n+1}) \\ \bar{x} &= X(t^{n+1}; x, t^n) \end{aligned} \tag{13}$$

So that (x, t^{n+1}) backtracks to (x^*, t^n) and (x, t^n) forward to $(\bar{x}, t^{n+1})$.

2.4. Definition of subdomains

In this work, we use a moving grid method. Therefore, subdomains are not fixed in space. The initial spatial discretization is fixed and the domain Ω is partitioned into nm different intervals $\Omega_i^0 = [x_{i-1/2}^0, x_{i+1/2}^0]$ centred at x_i^0. This discritization is used to compute the Darcy

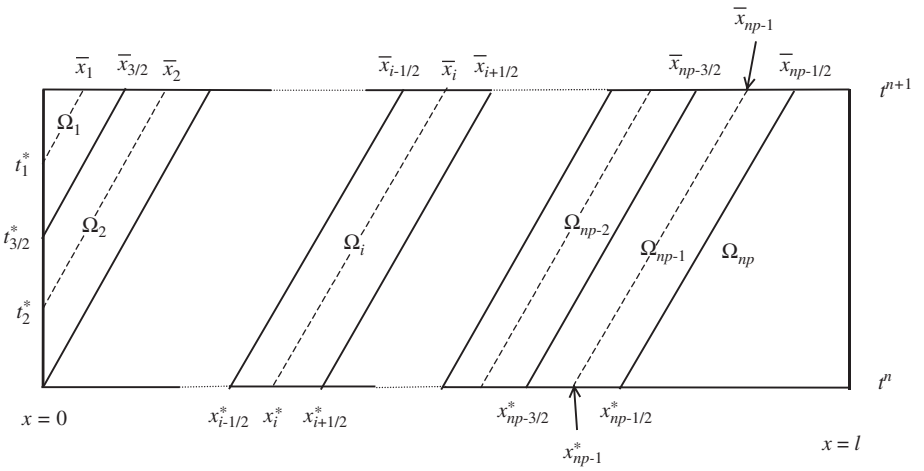

Figure 1. Definition of subdomains between t^n and t^{n+1}.

flux and the volumetric water content. We consider that subdomains Ω_i are dependent on the time step number and we set $\Omega_i = \Omega_i(\Delta t^{n+1})$.

For the first time step $\Delta t^1 = t^1 - t^0$: To define subdomains $\Omega_i(\Delta t^1)$, we compute $\bar{x}_i(\Delta t^1)$ and $\bar{x}_{i\pm1/2}(\Delta t^1)$ where $\bar{x}_i(\Delta t^1)$ (respectively $\bar{x}_{i\pm1/2}(\Delta t^1)$) is the location at $t = t^1$ obtained when forward tracking from x_i^0 (respectively $x_{i\pm1/2}^0$) at $t = t^0$.

For the other time steps $\Delta t^{n+1} = t^{n+1} - t^n$ *with* $n \geqslant 1$: To define $\Omega_i(\Delta t^{n+1})$ for each time step, we compute $\bar{x}_i(\Delta t^{n+1})$ and $\bar{x}_{i\pm1/2}(\Delta t^{n+1})$ where $\bar{x}_i(\Delta t^{n+1})$ (respectively $\bar{x}_{i\pm1/2}(\Delta t^{n+1})$) is the location at $t = t^{n+1}$ obtained when forward tracking from $x_i^0(\Delta t^{n+1})$ (respectively $x_{i\pm1/2}^*(\Delta t^{n+1})$) at $t = t^n$.

To avoid interpolation (which can be the origin of numerical diffusion [17]), the point at the foot of the characteristic between t^n and t^{n+1} corresponds to the point at the head of the characteristic between t^{n-1} and t^n:

$$\begin{aligned} x_i^*(\Delta t^{n+1}) &= \bar{x}_i(\Delta t^n) \\ x_{i\pm1/2}^*(\Delta t^{n+1}) &= \bar{x}_{i\pm1/2}(\Delta t^n) \end{aligned} \tag{14}$$

Inflow boundary: To take into account mass which enters the domain from the inflow boundary between t^n and t^{n+1}, we discretize the inflow boundary as shown in Figure 1. We add new points at the inflow boundary ($x_j^* = 0$) with different initial times ($t^n < t_j^* < t^{n+1}$) that we forward track to $\bar{x}_j > 0$ at $t = t^{n+1}$.

The number of these points depends on the behaviour of the boundary condition and/or the velocity near the inflow boundary. The spatial distribution of the final solution will also depend on the number of these points.

Let's assume that we split the time step Δt^{n+1} into p subintervals, p can depend on the non-uniform time step Δt^{n+1} and will be noted $p(\Delta t^{n+1})$. The number of subdomains Ω_i is then no longer constant, since for each time step Δt^{n+1}, we add $p(\Delta t^{n+1})$ new subdomains. The subdomain number has therefore to be adapted from one time step to another. For any

time step Δt^{n+1}, (14) has to be replaced by

$$\begin{aligned} x^*_{i+p(\Delta t^{n+1})}(\Delta t^{n+1}) &= \bar{x}_i(\Delta t^n) \\ x^*_{i+p(\Delta t^{n+1})\pm 1/2}(\Delta t^{n+1}) &= \bar{x}_{i\pm 1/2}(\Delta t^n) \end{aligned} \tag{15}$$

Outflow boundary: During Δt^{n+1} when forward tracking nodes from t^n to t^{n+1} some subdomains will intersect the outflow boundary.

If we assume that $r(\Delta t^{n+1})$ is the number of subdomains which arrive wholly at the outflow boundary, $np(\Delta t^{n+1})$ the total number of subdomains that reach partially or totally the spatial grid at t^{n+1}, we have:

$$\begin{aligned} np(\Delta t^{n+1}) &= np(\Delta t^n) + p(\Delta t^{n+1}) - r(\Delta t^{n+1}) \quad n \geqslant 1 \\ np(\Delta t^1) &= nm + p(\Delta t^1) - r(\Delta t^1) \end{aligned} \tag{16}$$

There are $np-1$ subdomains which start at $t^n < t < t^{n+1}$ in the inflow boundary or at $t = t^n$ in the spatial grid (Figure 1) and arrive wholly at the spatial grid at time $t = t^{n+1}$ when forward tracked.

2.5. Definition of the test and the trial functions

Let $x_{i\pm 1/2}(t)$ be the characteristic passing from $x^*_{i\pm 1/2}(\Delta t^{n+1})$ to $\bar{x}_{i\pm 1/2}(\Delta t^{n+1})$, the test function ω is defined as

$$\omega_i(x,t) = \begin{cases} 1 & x_{i-1/2}(t) < x < x_{i+1/2}(t), \quad t^n < t < t^{n+1} \\ 0 & \text{otherwise} \end{cases} \tag{17}$$

As in References [17, 24], the trial functions for C are chosen to be the piecewise linear basis functions

$$C = \sum_{i=1}^{np(\Delta t^{n+1})} C_i \phi_i \tag{18}$$

The nodes are located at the centres of the subdomains.

2.6. Derivation of equations

In the following $x^*_{i+1/2}(\Delta t^{n+1})$ and $\bar{x}_{i+1/2}(\Delta t^{n+1})$ will be denoted by $x^*_{i+1/2}$ and $\bar{x}_{i+1/2}$, respectively.

With the trial and test functions defined previously, the integrals in Equation (11) become (see Reference [2] for details)

$$\int_0^T \int_\Omega \frac{\partial(\theta \omega_i C)}{\partial t} \, \mathrm{d}x \, \mathrm{d}t = \int_{\bar{x}_{i-1/2}}^{\bar{x}_{i+1/2}} \theta^{n+1} C^{n+1} \, \mathrm{d}x - \int_{x^*_{i-1/2}}^{x^*_{i+1/2}} \theta^n C^n \, \mathrm{d}x \tag{19}$$

$$\int_0^T \int_\Omega D \frac{\partial C}{\partial x} \frac{\partial \omega_i}{\partial x} \, \mathrm{d}x \, \mathrm{d}t = \int_{t^*_{i-1/2}}^{t^{n+1}} D \frac{\partial C}{\partial x}\bigg|_{x_{i-1/2}(t)} \mathrm{d}t - \int_{t^*_{i+1/2}}^{t^{n+1}} D \frac{\partial C}{\partial x}\bigg|_{x_{i+1/2}(t)} \mathrm{d}t \tag{20}$$

$$\int_0^T \int_\Omega \left[\frac{\partial}{\partial x} \left(\left(qC - D \frac{\partial C}{\partial x} \right) \omega_i \right) \right] \mathrm{d}x \, \mathrm{d}t = \int_{\bar{t}_{i+1/2}}^{t^{n+1}} \left(qC - D \frac{\partial C}{\partial x} \right)_{x=l} \mathrm{d}t - \int_{t^*_{i+1/2}}^{t^*_{i-1/2}} \left(qC - D \frac{\partial C}{\partial x} \right)_{x=0} \mathrm{d}t \tag{21}$$

Notice that $t^*_{i+1/2}$ (respectively $\bar{t}_{i+1/2}$) is the time that the characteristic $x_{i+1/2}(t)$ intersects either the inflow (respectively the outflow) boundary of the domain or the time level t^n (respectively t^{n+1}).

The final ADE (11) leads to:

$$\int_{\bar{x}_{i-1/2}}^{\bar{x}_{i+1/2}} \theta^{n+1} C^{n+1} \, \mathrm{d}x + \int_{t^*_{i-1/2}}^{t^{n+1}} D \frac{\partial C}{\partial x}\bigg|_{x_{i-1/2}(t)} \mathrm{d}t - \int_{t^*_{i+1/2}}^{t^{n+1}} D \frac{\partial C}{\partial x}\bigg|_{x_{i+1/2}(t)} \mathrm{d}t - \int_{t^*_{i+1/2}}^{t^*_{i-1/2}} \left(qC - D \frac{\partial C}{\partial x} \right)_{x=0} \mathrm{d}t + \int_{\bar{t}_{i+1/2}}^{t^{n+1}} \left(qC - D \frac{\partial C}{\partial x} \right)_{x=l} \mathrm{d}t = \int_{x^*_{i-1/2}}^{x^*_{i+1/2}} \theta^n C^n \, \mathrm{d}x \tag{22}$$

A geometric interpretation of Equation (22) can be found in Reference [24].

3. NUMERICAL IMPLEMENTATION: PRIOR WORKS

All integrals in (22), with the exception of the integral on the right-hand side, are standard in finite elements and will be detailed in a later section. For the term on the right-hand side, the computational difficulties are due to the need to define the geometry at time t^n. The value of $C(x, t^n)$ is known from the solution at the previous time level but not $\omega_i(x, t^n) = \omega_i(\bar{x}, t^{n+1})$. Two approaches can be used to calculate this term.

The backtracking approach: In many characteristic and ELLAM works (for example, References [13, 21, 24, 25, 34, 35]), this term is written as an integral at time t^{n+1} using standard values of $\omega(x, t)$ and backtracking to time level n, where concentrations are known, to evaluate $C(x^*, t^n)$ by linear interpolation in x.

Results obtained by Binning [24] show that this approach can present numerical diffusion and/or oscillations when used for coarse discretizations. The mass lumping procedure allows us in this case to remove oscillations but increases numerical diffusion.

Numerical diffusion is added by interpolation errors introduced in the backtracking routine for non-integer Courant numbers.

Moreover, when using the backtracking approach, difficulties arise when the inflow boundary is intersected during backtracking [17]. Multidimensional problems require interpolation and mapping onto the fixed spatial grid at the previous time level which necessitates significant effort [36].

The forward-tracking approach: It was proposed by Russell and Trujillo [14] and was implemented by Healy and Russell for the one dimensional problem [17]. Rather than backtracking the geometry, discrete integration points x_p defined on the fixed grid at t^n can be forward tracked to $\bar{x}_p$ at time t^{n+1}, so that the amount of mass associated with x_p can be added to the corresponding position in the right-hand side in the global discrete linear algebraic system [37].

This approach was successfully used in one dimension by Healy and Russell [17]. They showed that using three integration points per cell is not sufficient to avoid numerical dispersion for all problems. To avoid this problem, they suggested using the trapezoidal rule and increasing the number of integration points per cell. For non-constant velocity and/or non-uniform grids, they suggested adding integration points at t^n at specific locations called strategic space integration points (SSIP). The locations of SSIPs are determined by backtracking from certain points on the grid from t^{n+1} to t^n. An important component of this method is to backtrack at the start of each time step from points in each cell where the slope of the test function changes [17].

Recently, a forward tracking ELLAM was used by Binning and Celia [38] for solution of the ADE in three dimensions. Each grid cell is covered with P integration points and known weights which are forward tracked to the new time level. However, one can notice that all simulations in Reference [38] are obtained for a single time step and if we use many time steps, this approach can also produce numerical diffusion as stated in Reference [17].

4. NUMERICAL IMPLEMENTATION: THE NEW ELLAM

We develop a new finite-volume Eulerian Lagrangian localized adjoint method using a moving spatial grid to define the solution and test functions of ELLAM. This avoids spatial interpolation, which is a major issue in conventional ELLAM formulations.

4.1. Evaluation of the integrals

We evaluate, in this section, all integrals given in Equations (2) and (22) and we give the final discrete system to solve in order to obtain the distribution of the concentration over the domain at each time step.

The fluid mass balance equation: The weak formulation of the fluid mass balance equation using the test function ω_i can be written as:

$$\int_\Omega \int_0^T \left[\frac{\partial \theta}{\partial t}\, \omega_i + \frac{\partial q}{\partial x}\, \omega_i \right] \mathrm{d}x\, \mathrm{d}t = 0 \tag{23}$$

which leads to

$$\int_\Omega \int_0^T \left[\frac{\partial (\omega_i \theta)}{\partial t} + \frac{\partial (\omega_i q)}{\partial x} \right] \mathrm{d}x\, \mathrm{d}t - \int_\Omega \int_0^T \left[\left(\theta\, \frac{\partial \omega_i}{\partial t} + q\, \frac{\partial \omega_i}{\partial x} \right) \right] \mathrm{d}x\, \mathrm{d}t = 0 \tag{24}$$

Since the space-time function ω_i is constant along the characteristics, we obtain

$$\int_\Omega \omega_i^{n+1} \theta^{n+1}\, \mathrm{d}x + \int_\Omega \int_0^T \frac{\partial (\omega_i q)}{\partial x}\, \mathrm{d}x\, \mathrm{d}t = \int_\Omega \omega_i^n \theta^n\, \mathrm{d}x \tag{25}$$

Using the definition (17), it leads to

$$\int_{\bar{x}_{i-1/2}}^{\bar{x}_{i+1/2}} \theta^{n+1}\,\mathrm{d}x + \int_{\bar{t}_{i+1/2}}^{t^{n+1}} q|_{x=l}\,\mathrm{d}t - \int_{t^*_{i+1/2}}^{t^*_{i-1/2}} q|_{x=0}\,\mathrm{d}t = \int_{x^*_{i-1/2}}^{x^*_{i+1/2}} \theta^n\,\mathrm{d}x \tag{26}$$

The mass lumping procedure: We use the mass lumping procedure for the system (22), the first term in the left-hand side becomes

$$\int_{\bar{x}_{i-1/2}}^{\bar{x}_{i+1/2}} C^{n+1}\theta^{n+1}\,\mathrm{d}x = C_i^{n+1}\int_{\bar{x}_{i-1/2}}^{\bar{x}_{i+1/2}} \theta^{n+1}\,\mathrm{d}x \tag{27}$$

where C_i^{n+1} is the unknown concentration at the new time level $n+1$ in $\bar{x}_i(\Delta t^{n+1})$.

The treatment of the term in the right-hand side gives

$$\int_{x^*_{i-1/2}}^{x^*_{i+1/2}} \theta^n C^n\,\mathrm{d}x = C_i^n \int_{x^*_{i-1/2}}^{x^*_{i+1/2}} \theta^n\,\mathrm{d}x \tag{28}$$

where C_i^n is the known concentration at the old time level n in $x_i^*(\Delta t^{n+1})$.

Notice that because we use a moving mesh, C_i^n and C_i^{n+1} do not refer to the same spatial location.

Evaluation of the dispersion terms: These integrals are line integrals along the characteristics and are evaluated using a one-step backward Euler approximation which gives:

$$\begin{aligned}\int_{t^*_{i-1/2}}^{t^{n+1}} D\,\frac{\partial C}{\partial x}\bigg|_{x_{i-1/2}(t)}\,\mathrm{d}t &\approx (t^{n+1}-t^*_{i-1/2})\left(D\,\frac{\partial C}{\partial x}\right)^{n+1}_{\bar{x}_{i-1/2}}\\ &= (t^{n+1}-t^*_{i-1/2})D^{n+1}_{\bar{x}_{i-1/2}}\left(\frac{C_i^{n+1}-C_{i-1}^{n+1}}{\bar{x}_i-\bar{x}_{i-1}}\right)\end{aligned} \tag{29}$$

$$\begin{aligned}\int_{t^*_{i+1/2}}^{t^{n+1}} D\,\frac{\partial C}{\partial x}\bigg|_{x_{i+1/2}(t)}\,\mathrm{d}t &\approx (t^{n+1}-t^*_{i+1/2})\left(D\,\frac{\partial C}{\partial x}\right)^{n+1}_{\bar{x}_{i+1/2}}\\ &= (t^{n+1}-t^*_{i+1/2})D^{n+1}_{\bar{x}_{i+1/2}}\left(\frac{C_{i+1}^{n+1}-C_i^{n+1}}{\bar{x}_{i+1}-\bar{x}_i}\right)\end{aligned} \tag{30}$$

Values of λ_L, q and θ are assumed to be known. Hence $D^{n+1}_{\bar{x}_{i-1/2}}$ can be approximated using values at $\bar{x}_{i-1/2}$. We can also approximate $D^{n+1}_{\bar{x}_{i-1/2}}$ averaging values at $\bar{x}_{i-1}, \bar{x}_{i-1/2}$ and $\bar{x}_i$.

4.2. Evaluation of integrals in (22) between t^n and t^{n+1} for central subdomains

This concerns all subdomains $\Omega_i = \Omega_i(\Delta t^{n+1})$ with

$$p(\Delta t^{n+1}) < i < n\,p(\Delta t^{n+1}) \tag{31}$$

For these subdomains, boundary integrals vanish and (22) becomes:

$$C_i^{n+1}\int_{\bar{x}_{i-1/2}}^{\bar{x}_{i+1/2}}\theta^{n+1}\,\mathrm{d}x+\int_{t_{i-1/2}^*}^{t^{n+1}}D\left.\frac{\partial C}{\partial x}\right|_{x_{i-1/2}(t)}\mathrm{d}t-\int_{t_{i+1/2}^*}^{t^{n+1}}D\left.\frac{\partial C}{\partial x}\right|_{x_{i+1/2}(t)}\mathrm{d}t=C_i^n\int_{x_{i-1/2}^*}^{x_{i+1/2}^*}\theta^n\,\mathrm{d}x \tag{32}$$

Equation (26) gives for central subdomains

$$\bar{\bar{\theta}}_i^{n+1}=\int_{\bar{x}_{i-1/2}}^{\bar{x}_{i+1/2}}\theta^{n+1}\,\mathrm{d}x=\int_{x_{i-1/2}^*}^{x_{i+1/2}^*}\theta^n\,\mathrm{d}x \tag{33}$$

using the following notation:

$$\alpha_1=-\frac{D_{\bar{x}_{i-1/2}}^{n+1}}{\bar{\bar{\theta}}_i^{n+1}}\left(\frac{t^{n+1}-t_{i-1/2}^*}{\bar{x}_i-\bar{x}_{i-1}}\right) \tag{34}$$

$$\beta_1=-\frac{D_{\bar{x}_{i+1/2}}^{n+1}}{\bar{\bar{\theta}}_i^{n+1}}\left(\frac{t^{n+1}-t_{i+1/2}^*}{\bar{x}_{i+1}-\bar{x}_i}\right) \tag{35}$$

The ADE written for central subdomains leads to

$$\alpha_1 C_{i-1}^{n+1}+(1-\alpha_1-\beta_1)C_i^{n+1}+\beta_1 C_{i+1}^{n+1}=C_i^n \tag{36}$$

4.3. Evaluation of integrals in (22) between t^n and t^{n+1} for subdomains starting at the inflow boundary

This concern all subdomains $\Omega_i=\Omega_i(\Delta t^{n+1})$ with

$$i\leqslant p(\Delta t^{n+1}) \tag{37}$$

For these subdomains, we have to evaluate the following boundary integral

$$\int_{t_{i+1/2}^*}^{t_{i-1/2}^*}\left(qC-D\frac{\partial C}{\partial x}\right)_{x=0}\mathrm{d}t \tag{38}$$

Dirichlet boundary condition: If we assume a Dirichlet boundary condition $C(0,t)=g_1(t)$ at the inflow boundary, (38) becomes

$$\int_{t_{i+1/2}^*}^{t_{i-1/2}^*}\left(qC-D\frac{\partial C}{\partial x}\right)_{x=0}\mathrm{d}t=\int_{t_{i+1/2}^*}^{t_{i-1/2}^*}(qC)_{x=0}\,\mathrm{d}t-\int_{t_{i+1/2}^*}^{t_{i-1/2}^*}\left(D\frac{\partial C}{\partial x}\right)_{x=0}\mathrm{d}t \tag{39}$$

The time interval Δt^{n+1} is divided to obtain $p(\Delta t^{n+1})$ subdomains. If we assume $g_1(t)=g_1(t_i^*)$ constant over the interval $[t_{i+1/2}^*,t_{i-1/2}^*]$, then

$$\int_{t_{i+1/2}^*}^{t_{i-1/2}^*}(qC)_{x=0}\,\mathrm{d}t=g_1(t_i^*)\int_{t_{i+1/2}^*}^{t_{i-1/2}^*}q|_{x=0}\,\mathrm{d}t \tag{40}$$

The dispersion term is approximated using a one-step backward Euler approximation:

$$\int_{t^*_{i+1/2}}^{t^*_{i-1/2}} \left(D \frac{\partial C}{\partial x} \right)\Big|_{x=0} \mathrm{d}t \approx (t^*_{i-1/2} - t^*_{i+1/2}) D \left. \frac{\partial C}{\partial x} \right|^{n+1}_{x=\bar{x}_i}$$

$$= (t^*_{i-1/2} - t^*_{i+1/2}) \left[\frac{D^{n+1}_{\bar{x}_{i-1/2}}}{2} \left(\frac{C^{n+1}_i - C^{n+1}_{i-1}}{\bar{x}_i - \bar{x}_{i-1}} \right) + \frac{D^{n+1}_{\bar{x}_{i+1/2}}}{2} \left(\frac{C^{n+1}_{i+1} - C^{n+1}_i}{\bar{x}_{i+1} - \bar{x}_i} \right) \right] \tag{41}$$

The fluid mass balance (26) simplifies to:

$$\bar{\bar{\theta}}^{n+1}_i = \int_{\bar{x}_{i-1/2}}^{\bar{x}_{i+1/2}} \theta^{n+1} \mathrm{d}x = \int_{t^*_{i+1/2}}^{t^*_{i-1/2}} q|_{x=0} \mathrm{d}t \tag{42}$$

The ADE (22) written for subdomains $\Omega_i = \Omega_i(\Delta t^{n+1})$ with $i \leqslant p(\Delta t^{n+1})$ becomes:

$$(\alpha_0 + \alpha_1) C^{n+1}_{i-1} + (1 - \alpha_0 - \beta_0 - \alpha_1 - \beta_1) C^{n+1}_i + (\beta_0 + \beta_1) C^{n+1}_{i+1} = g_1(t^*_i) \tag{43}$$

where α_1 and β_1 are still defined by (34), (35) and α_0 and β_0 given by

$$\alpha_0 = -\frac{D^{n+1}_{\bar{x}_{i-1/2}}}{2\bar{\bar{\theta}}^{n+1}_i} \left(\frac{t^*_{i-1/2} - t^*_{i+1/2}}{\bar{x}_i - \bar{x}_{i-1}} \right), \quad \beta_0 = \frac{D^{n+1}_{\bar{x}_{i+1/2}}}{2\bar{\bar{\theta}}^{n+1}_i} \left(\frac{t^*_{i-1/2} - t^*_{i+1/2}}{\bar{x}_{i+1} - \bar{x}_i} \right) \tag{44}$$

Total flux boundary condition $(qC(0,t) - D\partial C(0,t)/\partial x) = g_3(t)$: Assuming $g_3(t^*_i)$ the constant value of $g_3(t)$ for $t^*_{i+1/2} \leqslant t \leqslant t^*_{i-1/2}$, the boundary integral is approximated as following

$$\int_{t^*_{i+1/2}}^{t^*_{i-1/2}} \left(qC - D \frac{\partial C}{\partial x} \right)_{x=0} \approx (t^*_{i-1/2} - t^*_{i+1/2}) g_3(t^*_i) \tag{45}$$

The ADE (22) becomes:

$$\alpha_1 C^{n+1}_{i-1} + (1 - \alpha_1 - \beta_1) C^{n+1}_i + \beta_1 C^{n+1}_{i+1} = \frac{(t^*_{i-1/2} - t^*_{i+1/2})}{\bar{\bar{\theta}}^{n+1}_i} g_3(t^*_i) \tag{46}$$

4.4. Evaluation of integrals in (22) between t^n and t^{n+1} for the last subdomain which crossed the outflow boundary

For the last subdomain Ω_{np}, Equation (22) with no dispersive outflow is

$$C^{n+1}_{np} \int_{\bar{x}_{np-1/2}}^{l} \theta^{n+1} \mathrm{d}x + \int_{t^n}^{t^{n+1}} qC|_{x=l} \mathrm{d}t + \int_{t^n}^{t^{n+1}} D \left. \frac{\partial C}{\partial x} \right|_{x_{np-1/2}(t)} \mathrm{d}t = \int_{x^*_{np-1/2}}^{l} \theta^n C^n \mathrm{d}x \tag{47}$$

The fluid balance equation gives

$$\bar{\bar{\theta}}^n_{np} = \int_{x^*_{np-1/2}}^{l} \theta^n \mathrm{d}x = \int_{\bar{x}_{np-1/2}}^{l} \theta^{n+1} \mathrm{d}x + \int_{t^n}^{t^{n+1}} q|_{x=l} \mathrm{d}t \tag{48}$$

The dispersive outflow is zero, then

$$C(l,t) = C_{np+1/2} = C_{np} \tag{49}$$

Equation (47) leads to

$$C_{np}^{n+1} + \frac{D_{\bar{x}_{i-1/2}}^{n+1}}{\bar{\bar{\theta}}_{np}^{n}} \left(\frac{\Delta t^{n+1}}{\bar{x}_{np} - \bar{x}_{np-1}} \right) (C_{np}^{n+1} - C_{np-1}^{n+1}) = \frac{1}{\bar{\bar{\theta}}_{np}^{n}} \left(\int_{x_{np-1/2}^{*}}^{l} \theta^n C^n \, \mathrm{d}x \right) \tag{50}$$

where

$$\int_{x_{np-1/2}^{*}}^{l} \theta^n C^n \, \mathrm{d}x = \sum_{i=np}^{np+r(\Delta t^{n+1})} C_i^n \int_{x_{i-1/2}^{*}}^{x_{i+1/2}^{*}} \theta^n \, \mathrm{d}x \tag{51}$$

using, the notation

$$\alpha_3 = \frac{D_{\bar{x}_{i-1/2}}^{n+1}}{\bar{\bar{\theta}}_{np}^{n}} \left(\frac{\Delta t^{n+1}}{\bar{x}_{np} - \bar{x}_{np-1}} \right) \quad \gamma = \frac{1}{\bar{\bar{\theta}}_{np}^{n}} \left(\sum_{i=np}^{np+r(\Delta t^{n+1})} C_i^n \int_{x_{i-1/2}^{*}}^{x_{i+1/2}^{*}} \theta^n \, \mathrm{d}x \right) \tag{52}$$

the ADE written for the last domain Ω_{np} can then be written as:

$$-\alpha_3 C_{np-1}^{n+1} + (1 + \alpha_3) C_{np}^{n+1} = \gamma \tag{53}$$

5. NUMERICAL RESULTS

To study the accuracy of the ELLAM formulation presented, we simulate, in this part, the transport of solute in both saturated and unsaturated porous medium with different spatial and time discretizations. We compare our numerical results to analytical solution, Binning ELLAM results (given in Reference [24]), Standard Finite Element and Discontinuous Finite Element Results. To obtain the numerical solution, we solve the linear system of equations formed by Equations (36), (43) and (53). We obtain a tridiagonal system which can be easily solved.

5.1. The constant coefficients ADE

Before comparing the different numerical schemes, let's study the behaviour of the ELLAM solution when varying the time step size and/or the number of added subdomains at the inflow boundary.

Indeed, we noticed that in order to take into account the mass which enters the domain from the inflow boundary between t^n and t^{n+1}, we have to add inflow boundary subdomains during each time step. The solution and also the computational cost are dependent on the number $p(\Delta t^{n+1})$ of added subdomains per time step. For practical problems, $p(\Delta t^{n+1})$ can be related to the CFL number as done in Reference [38]. For constant velocity and time step size, the number of added subdomains is fixed and noted $p(\Delta t^{n+1}) = \hat{p}$. However, in this case and even for regular meshes, the number $r(\Delta t^{n+1})$ of subdomains, leaving the domain from the outflow boundary between t^n and t^{n+1}, is not constant. Let's note $\hat{r}$ the average value of $r(\Delta t^{n+1})$ for many time steps.

Table I. The error with the developed ELLAM for different cases of added inflow subdomains.

	Time step size	Number of time steps	Final number of subdomains	Error
Case 1 ($\hat{p}=1>\hat{r}$)	10	50	75	2.4×10^{-3}
Case 2 ($\hat{p}=7>\hat{r}$)	50	10	95	2.6×10^{-3}
Case 3 ($\hat{p}=3\approx\hat{r}$)	50	10	55	2.7×10^{-3}
Case 4 ($\hat{p}=1<\hat{r}$)	50	10	35	4.1×10^{-3}
Case 5 ($\hat{p}=\hat{r}=26$)	500	1	50	8.2×10^{-3}

At each time step, we add at least one subdomain at the inflow boundary and we always have $\hat{p}\geqslant 1$.

Since subdomains near the outflow boundary can be larger than those added at the inflow boundary, for small time steps we have $\hat{p}=1$ and $\hat{r}<1$. In this case, during simulation we have many more added subdomains at the inflow boundary then disappearing subdomains at the outflow boundary. This implies that during simulation, the initial mesh is replaced by a finer one, which arrives progressively from the inflow boundary (which corresponds to case 1).

Notice that increasing the time step size allows more flexibility when choosing the number of added subdomains. If we assume $\hat{r}\geqslant 1$, we can choose the number $\hat{p}$ of added subdomains such that:

- Case 2: $\hat{p}>\hat{r}$, this case is similar to case 1.
- Case 3: $\hat{p}\approx\hat{r}$, thus during each time step the number of added subdomains is close to the number of disappearing subdomains. This allows us to keep the mesh and the computational cost per time step constant.
- Case 4: $\hat{p}<\hat{r}$, thus the number of added inflow boundary subdomains is less than the number of disappearing subdomains at the outflow boundary. This implies that during simulation, the initial mesh is replaced by a coarser one which arrives progressively from the inflow boundary.

To study the behaviour and the accuracy of the numerical solution for the four stated cases, we simulate the progress of a concentration front in an infinite column of saturated porous medium. The analytical solution is given in Reference [29].

The problem is solved for different Peclet and CFL numbers with boundary conditions $C(0,t)=1, C(\infty,t)=0$ and initial condition $C(x,0)=0$ for $x>0$.

The domain is composed of a uniform grid, with $\Delta x=20$ and $l=1000$ which corresponds to 50 initial subdomains. The parameters are $q(x,t)=1$, $\theta(x,t)=1$, and $\lambda_L=2$ which corresponds to $P_e=10$. The final simulation time is 500. For each case, Table I gives the time step size, the number of time steps, the final number of subdomains and the error of the solution defined as

$$\text{error}=\frac{1}{np}\sum_{i=1}^{np}|C_i^{\text{numerical}}-C^{\text{analytical}}(x_i)|$$

Case 5 in Table I corresponds to the case of a single time step of 500.

The distribution of concentration over the domain at $t=500$ for all previous cases is given in Figure 2(a)–2(e).

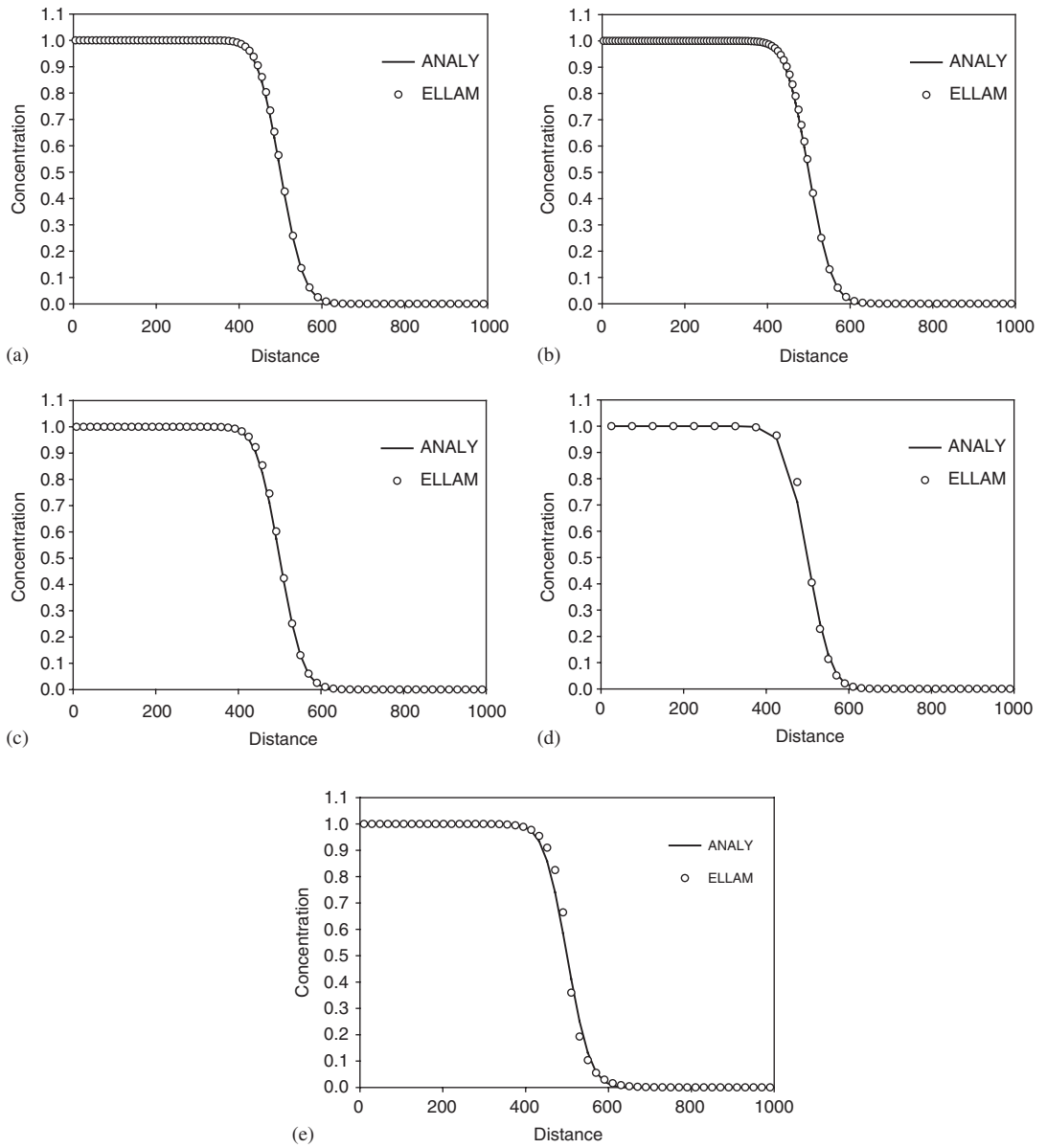

Figure 2. Concentration at $t = 500$ for (a) case 1, (b) case 2, (c) case 3, (d) case 4 and (e) case 5.

Table I shows that the more accurate results are obtained for cases with a finer final grid ($\hat{p} > \hat{r}$). When only one time step is used, the ELLAM under-predicts the physical dispersion as observed in Reference [38].

All errors in Table I are relatively small, but to assess the contribution of ELLAM, these errors have to be compared to those obtained with the commonly used numerical methods

Table II. Error with different numerical methods.

	FEM	DFEM	ELLAM
CFL = 1, $Pe = 1$	2.6×10^{-2}	7×10^{-3}	4.8×10^{-3}
CFL = 0.5, $Pe = 200$	4.8×10^{-2}	1.8×10^{-2}	2.2×10^{-3}

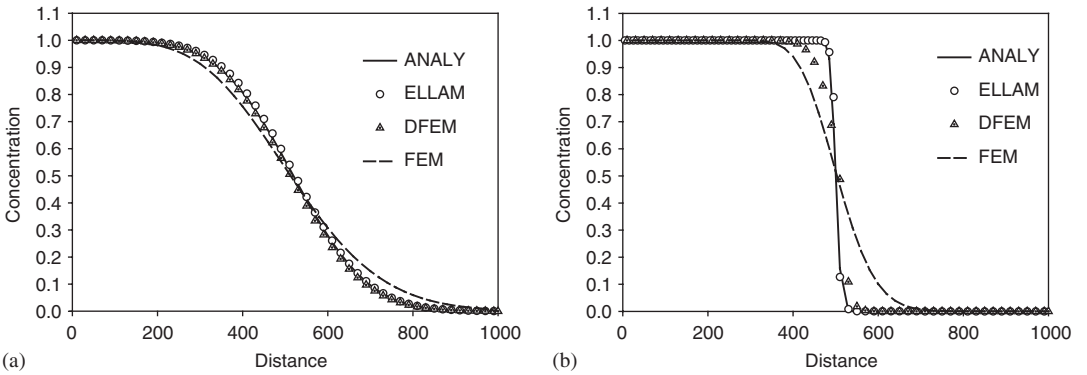

Figure 3. Concentration at $t = 500$ with different numerical methods for (a) CFL = 1 and $Pe = 1$, (b) CFL = 0.5 and $Pe = 200$.

when solving the ADE. With this aim, the same example is used to compare errors of the following methods:

- Eulerian method: the implicit Galerkin finite element method with linear basis and test functions.
- High-order Eulerian method: the discontinuous finite element method given in Reference [33]. In this case, the transport equation is solved using operator splitting with DFEM for discretization of the advective term and implicit standard FEM for discretization of the dispersive term.
- The developed ELLAM.

We simulate two cases corresponding to CFL = 1, $Pe = 1$ and CFL = 0.5, $Pe = 200$. In order to keep the same mesh and computational cost per time step, we choose for both cases $\hat{p}$ close to $\hat{r}$.

Results given in Table II and Figures 3(a) and 3(b) show that the ELLAM is the more accurate method. We have done many other numerical experiments with a large range of CFL and Peclet numbers. In all cases, the ELLAM gives the most accurate results.

The DFEM gives good results for CFL = 1. For CFL less than one, it introduces some numerical diffusion. This method cannot be used for CFL greater than one, since it uses an explicit time discretization for the advection equation. This restriction could make DFEM very expensive for non-uniform grid. Indeed, if we assume that in the above domain there is only one element which is 100 times smaller than all other elements, the CFL restriction implies

Table III. Parameters and boundary conditions for the unsaturated problem.

Domain length	$l = 20$ cm
Initial condition for flow	$h(z,0) = -100$ cm
Boundary conditions for flow	$q_0(z=0,t) = 8.3$ cm/h (upper: Neumann)
	$h(z=l,t) = -100$ cm (lower: Dirichlet)
Parameters for flow	Van Genuchten parameters:
	$\theta_s = 0.312,\ \theta_r = 0.0265,\ \alpha = 0.04\ \text{cm}^{-1},\ n = 2.2$
	Conductivity function
	$K = A\theta^B$ ($A = 18130$ cm/h and $B = 6.07$).
	$\Delta z = 1$ cm, $\Delta t = 1$ s
Initial condition for transport	$C(z,0) = 0$
Boundary conditions for transport	$C(z=0,t) = 1$ (upper: Dirichlet)
	$(\partial C/\partial z)_{z=l} = 0$ (lower: no dispersive flux)
Parameters for transport	$\lambda_L = 0.1$ cm
	$D_m = 0$
	$\Delta t = 1,\ 100$ and 1000 s

a computational effort which is 100 times greater than for the previous study. ELLAM can avoid this drawback and involves similar work for both cases.

5.2. *The variable coefficients ADE*

We are now interested in transport in the unsaturated porous medium. In this case velocity and water content are no longer constant in time. In order to compare our ELLAM method to previous work, we simulate the problem described in Reference [24].

A 20 cm column contains Touma and Vauclin [39] coarse sand and the boundary conditions for flow are a flux of $8.3\,\text{cm}\,\text{h}^{-1}$ water on the surface, and a fixed head of -100 cm of water on the bottom of the column, corresponding to a uniform initial condition (see Table III). The air phase is assumed to present large mobility and is considered at atmospheric pressure. As in Reference [24], we use a uniform time step of size $\Delta t = 1$ s and a uniform spatial discretization of $\Delta z = 1$ cm for the flow problem. Following Celia *et al.* [40], we solve the flow equation using the mixed form of the Richards equation:

$$\frac{\partial \theta}{\partial t} - \frac{\partial}{\partial z}\left[K(h)\frac{\partial h}{\partial z}\right] + \frac{\partial K}{\partial z} = 0 \tag{54}$$

with h the pressure head and $K(h)$ is unsaturated hydraulic conductivity.

Equation (54) is obtained from the fluid mass balance equation (2), written for the vertical column and the Darcy's velocity which is

$$q = -K(h)\nabla(h - z) = -K(h)\left(\frac{\partial h}{\partial z} - 1\right) \tag{55}$$

where the z-axis is oriented downward.

The empirical Van Genuchten [41] pressure saturation relation used is

$$\theta = \frac{\theta_s - \theta_r}{|1 + (\alpha h)^n|^{1-1/n}} + \theta_r \tag{56}$$

where $\theta_s, \theta_r, \alpha, n$ are fitting parameters given by Touma and Vauclin [39]:

$$\theta_s = 0.312, \quad \theta_r = 0.0265, \quad \alpha = 0.044\ \mathrm{cm}^{-1}, \quad n = 2.2 \tag{57}$$

Denoting $S(h) \equiv \mathrm{d}\theta/\mathrm{d}h$ the specific moisture capacity function and using standard finite difference for the modified Picard approximation [40] of (54) leads to:

$$\begin{aligned} S_i^{n+1,m} \frac{\delta_i^m}{\Delta t} - \frac{1}{(\Delta z)^2}[K_{i+1/2}^{n+1,m}(\delta_{i+1}^m - \delta_i^m) - K_{i-1/2}^{n+1,m}(\delta_i^m - \delta_{i-1}^m)] \\ = \left(\frac{K_{i+1/2}^{n+1,m}(h_{i+1}^{n+1,m} - h_i^{n+1,m}) - K_{i-1/2}^{n+1,m}(h_i^{n+1,m} - h_{i-1}^{n+1,m})}{(\Delta z)^2} \right) \\ - \left(\frac{K_{i+1/2}^{n+1,m} - K_{i-1/2}^{n+1,m}}{\Delta z} \right) - \left(\frac{\theta_i^{n+1,m} - \theta_i^n}{\Delta t} \right) \end{aligned} \tag{58}$$

where m is the iteration level and $\delta_i^m = h_i^{n+1,m+1} - h_i^{n+1,m}$.

The water conductivity function of Touma and Vauclin [39] is described with the fitted curve:

$$K = A\theta^B \tag{59}$$

with $A = 18130\ \mathrm{cm/h}$ and $B = 6.07$.

For the transport equation, the velocity and water content are no longer constant either in space or in time. Their spatial distributions are obtained at each time step by first solving the flow equation. Figure 4(a) shows the volumetric water content distribution in the column at $t = 1000$ s.

In this study, a boundary condition of $C = 1.0$ is used at the top and $C = 0.0$ corresponding to the initial condition, at the bottom. The dispersivity is set to $\lambda_L = 0.1$ cm.

This problem was studied by Binning [24] with both ELLAM and FE methods for a variety of time steps. Three simulations with different time steps ($\Delta t = 1$ s, 100 s and 1000 s) are carried out with the current ELLAM method (Table IV). Since the velocity downstream of the infiltration front is essentially zero, we have for all simulations $\hat{r} = 0$. The final number of subdomains becomes significant if we add many subdomains at each time step or when using a very small time step as in simulation 1. For simulations 2 and 3, we choose to add only 10 and 6 subdomains respectively at the inflow boundary. For both cases, we obtain a coarse final discretization of respectively 30 and 26 subdomains.

Recall that for this non-constant ADE, our ELLAM corresponds to the non-conservative form given in [25]. Indeed, the cumulative mass balance ratio defined by

$$\text{cumulative mass balance ratio} = \frac{\int_\Omega \theta^{n+1} C^{n+1}\,\mathrm{d}x - \int_\Omega \theta^0 C^0\,\mathrm{d}x}{\int_0^T \left(qC - D\frac{\partial C}{\partial x} \right)_{x=l} \mathrm{d}t - \int_0^T \left(qC - D\frac{\partial C}{\partial x} \right)_{x=0} \mathrm{d}t}$$

is illustrated in Figure 4(b) for the simulation 1. As stated in Binning [24], the mass balance error is significant at the beginning of the simulation, but the method improves at later times. The origin of these errors is explained in References [24, 25].

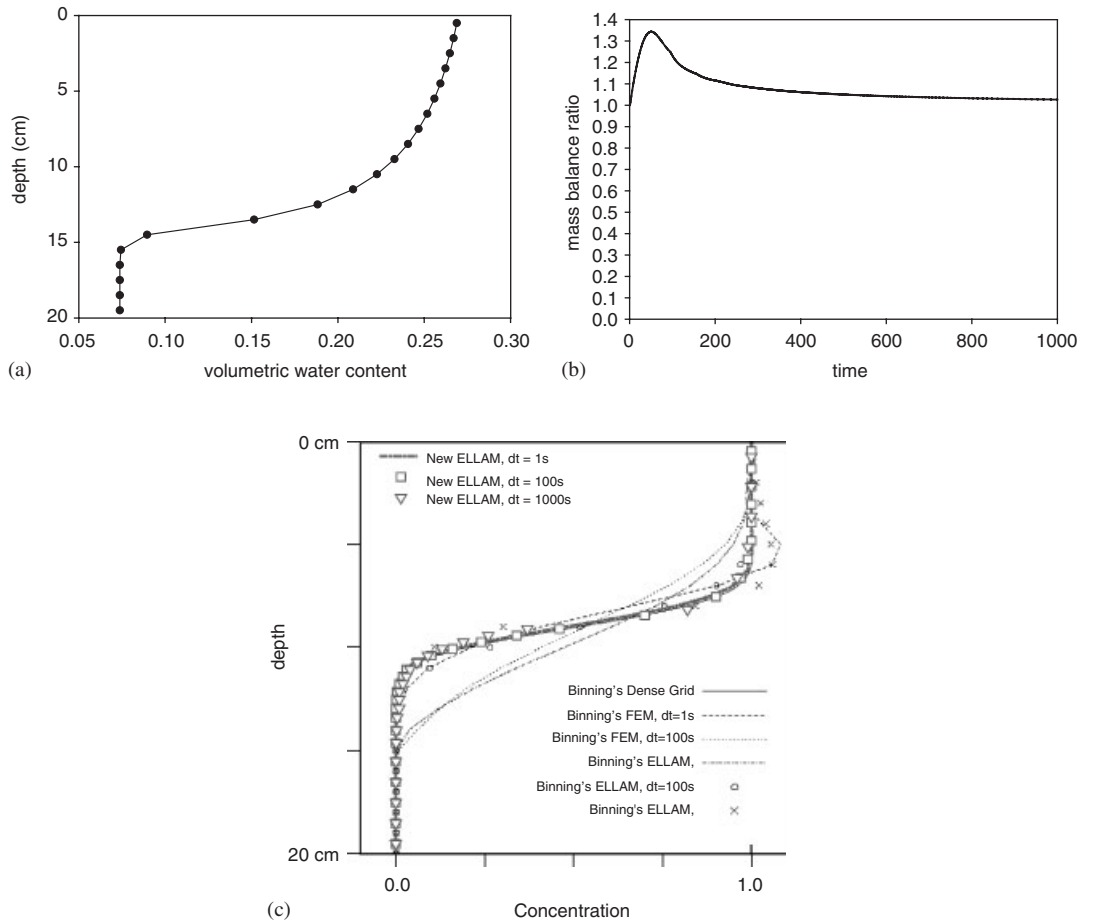

Figure 4. (a) Distribution of θ in the column at $t = 1000$ s, (b) Cumulative mass balance error for simulation 1. (c) Finite element, binning ELLAM and current ELLAM results with varying time step size after 1000 s of simulation time for the unsaturated case (FE and binning ELLAM results are extracted from Reference [6]).

In Figure 4(c), we add results of simulations 1, 2 and 3 to the FE and ELLAM results of Binning [24]. All results are obtained at a simulation time of 1000 s. This figure shows the accuracy of the new ELLAM, since with all time step sizes and even when using a single time step ($\Delta t = 1000$ s) and a coarse grid of 26 subdomains, results are very close to the dense grid results of Binning [24].

6. CONCLUSION

In this work, we have developed a new finite-volume Eulerian Lagrangian localized adjoint method based on a forward tracking procedure. To avoid spatial interpolation, or

Table IV. Description of the 3 simulations for the unsaturated problem.

	Time step size	Number of time steps	Added subdomains per time step ($\hat{p}$)	Final number of subdomains
Simulation 1	1	1000	1	1020
Simulation 2	100	10	1	30
Simulation 3	1000	1	6	26

equivalently numerical integration, which is a major issue in conventional ELLAM formulations, the method uses a moving grid to define the solution and test functions.

This method is used to simulate transport of solute in both saturated and unsaturated porous medium for a large range of CFL and grid Peclet numbers. Numerical results of ELLAM for constant coefficient ADE are shown to be more accurate than those of the commonly used numerical methods. For variable coefficient ADE, results show the superiority of the presented method compared to prior ELLAM formulations.

NOMENCLATURE

$C(x,t)$	concentration (ML^{-3})
$q(x,t)$	Darcy's velocity (LT^{-1})
$\theta(x,t)$	volumetric water content
$D(x,t)$	dispersion coefficient (L^2T^{-1})
λ_L	longitudinal pore-scale dispersivity (L)
D_m	molecular diffusion coefficient in free water (L^2T^{-1})
τ	tortuosity factor
θ_S	saturation water content
$L(C)$	differential operator
Ω_{xt}	spatial-time domain
Ω	spatial domain
$\partial\Omega$	domain boundary
$n_{\partial\Omega}$	outward unit normal on $\partial\Omega$
t, T	time (T)
l	length of the domain (L)
nm	initial number of subdomains
Ω_i^0	initial subdomain
Δx_i	length of subdomain (L)
Δt^{n+1}	time interval $\Delta t^{n+1} = t^{n+1} - t^n$ (T)
n	time index
$\omega(x,t)$	space-time test function
$V(x,t)$	fluid velocity (LT^{-1})
X	tracked location of point (L)
x^*	backtracked coordinate at t^n (L)
$\bar{x}$	forward tracked coordinate at t^{n+1} (L)
$\Omega_i(\Delta t^{n+1})$	subdomain Ω_i; its location depend on the time step number

$p(\Delta t^{n+1})$	number of inflow subintervals for Δt^{n+1}
$r(\Delta t^{n+1})$	number of subdomains which arrive wholly at the outflow for Δt^{n+1}
$np(\Delta t^{n+1})$	total number of subdomains that reach partially or totally the spatial grid at t^{n+1}
C_i^{n+1}	unknown concentration at the new time level $n+1$ in $\bar{x}_i(\Delta t^{n+1})$
$\hat{p}$	average value of $p(\Delta t^{n+1})$
$\hat{r}$	average value of $r(\Delta t^{n+1})$ for many time steps
P_e	grid Peclet number
h	pressure head (L)
$K(h)$	unsaturated hydraulic conductivity (LT^{-1})
$\theta_s, \theta_r, \alpha, n$	fitting parameters
$S(h)$	specific moisture capacity function (L^{-1})
m	iteration level

REFERENCES

1. Peyret R, Taylor TD. *Computational Methods for Fluid Flow*. Springer: New York, 1983.
2. Van Leer B. Towards the ultimate conservative scheme: a second order sequel to Godunov's method. *Journal of Computational Physics* 1979; **32**:101–136.
3. Roe PL. Characteristic-based schemes for the Euler equation. *Annual Review of Fluid Mechanics* 1986; **18**: 337–365.
4. Ewing RE, Wang H. A summary of numerical methods for time-dependent advection-dominated partial differential equations. *Journal of Computers and Applied Mathematics* 2001; **128**:423–445.
5. Cirpka OA, Helmig R, Frind EO. Numerical methods for reactive transport on rectangular and streamline-oriented grids. *Advances in Water Resources* 1999a; **227**:697–710.
6. Hoteit H, Mose R, Younes A, Lehmann F, Ackerer Ph. Three dimensional modeling of mass transfer in porous media using the mixed hybrid finite elements and the random walk methods. *Mathematical Geology* 2002; **34**:435–456.
7. Yeh GT, Chang JR, Short TE. An exact peak capturing and oscillation-free scheme to solve advection-dispersion transport equations. *Water Resources Research* 1992; **28**:2937–2951.
8. Benque JP, Ronat J. Quelques difficultés des modèles numériques en hydraulique. In *Computing Methods in Applied Sciences and Engineering*, Glowinski, Lions (eds). North-Holland: Amsterdam, 1982; 471–494.
9. Douglas Jr J, Russell TF. Numerical methods for convection-dominated diffusion problems based on combining the method of characteristics with finite element or finite difference procedures. *SIAM Journal of Numerical Analysis* 1982; **19**(5):871–885.
10. Garder AO, Peaceman DW, Pozzi AL. Numerical calculations of multidimensional miscible displacement by the method of characteristics. *Society of Petroleum Engineers Journal* 1964; **4**:26–36.
11. Neuman SP. An Eulerian–Lagrangian numerical scheme for the dispersion-convection equation using conjugate space-time grids. *Journal of Computational Physics* 1981; **41**:270–294.
12. Pollock DW. Semi analytical computation of path lines for finite difference models. *Ground Water* 1988; **26**: 743–750.
13. Celia MA, Russell TF, Herrera I, Ewing RE. An Eulerian–Lagrangian localized adjoint method for the advection-diffusion equation. *Advances in Water Resources* 1990; **13**:187–206.
14. Russell TF, Trujillo RV. Eulerian–Lagrangian localized adjoint methods with variable coefficients in multiple dimensions. Computational methods in surface hydrology. *Proceedings of the Eighth International Conference on Computational Methods in Water Resources*, Venice, Italy, 1990; 357–363.
15. Wang H, Ewing RE, Russell TF. Eulerian–Lagrangian localized methods for convection-diffusion equations and their convergence analysis. *IMA Journal of Numerical Analysis* 1995; **15**:4050–4059.
16. Celia MA, Ferrand IA. A comparison of ELLAM formulations for simulation of reactive transport in groundwater. In *Advances in Hydro-Science and Engineering*, Wang (ed.), vol. 1(B). University of Mississippi Press, MS, USA, 1993; 1829–1836.
17. Healy RW, Russell TF. A finite-volume Eulerian–Lagrangian localized adjoint method for solution of the advection-dispersion equation. *Water Resources Research* 1993; **29**:2399–2413.
18. Arbogast T, Wheeler MF. A characteristics-mixed finite element method for advection-dominated transport problems. *SIAM Journal of Numerical Analysis* 1995; **32**:404–424.

19. Celia MA, Zisman S. An Eulerian–Lagrangian localized adjoint method for reactive transport in groundwater. In *Conference on Computational Methods in Water Resources VIII*, Gambolati G *et al.* (eds), vol. I. Springer: Berlin, 1990; 383–392.
20. Vag JE, Wang H, Dahle HK. Eulerian–Lagrangian localized adjoint methods for systems of nonlinear advective-diffusive-reactive equations. *Advances in Water Resources* 1996; **19**:297–315.
21. Ewing RE, Wang H. Eulerian–Lagrangian localized adjoint methods for variable-coefficient advective-diffusive-reactive equations in groundwater contaminant transport. In *Advances in Optimization and Numerical Analysis, Mathematics and Its Applications*, Gomez, Hennart (eds), vol. 275. Kluwer Academic Publishers: Dordrecht, Netherlands, 1994; 185–205.
22. Wang H, Ewing RE, Qin G, Lyons SL, Al-Lawatia M, Man S. A family of Eulerian–Lagrangian localized adjoint methods for multi-dimensional advection-reaction equations. *Journal of Computational Physics* 1999; **152**:120–163.
23. Wang H, Sharpley RC, Man S. An ELLAM scheme for advection-diffusion equations in multidimensions. In *Computational Methods in Water Resources XI*, Aldama A *et al.* (eds). Computational Mechanics Publications: Southampton, Boston, 1996; 99–106.
24. Binning P. Modeling unsaturated zone flow and contaminant in the air and water phases. *Ph.D. Thesis*, Department of Civil Engineering and Operational Research, Princeton University, Princeton, NJ, 1994.
25. Binning P, Celia MA. A finite volume Eulerian–Lagrangian localized adjoint method for solution of the contaminant transport equations in two-dimensional multi-phase flow systems. *Water Resources Research* 1996; **32**:103–114.
26. Healy RW, Russell TF. Solution of the advection-dispersion equation in two dimensions by a finite-volume Eulerian–Lagrangian localized adjoint method. *Advances in Water Resources* 1998; **21**:11–26.
27. Weizhang H, Zheng L, Zhan X. Adaptative moving methods for simulating one-dimensional groundwater problems with sharp moving fronts. *International Journal for Numerical Methods in Engineering* 2002; **54**: 1579–1603.
28. Zheng C, Bennett GD. *Applied Contaminant Transport Modelling*: *Theory and Practice*. Van Nostrand Reinhold: New York, 1995.
29. Bear J. *Hydraulics of Groundwater*. McGraw-Hill: New York, 1979.
30. Maraqa MA, Wallace RB, Voice TC. Effects of degree of water saturation on dispersivity and immobile water in sandy soil columns. *Journal of Contaminant Hydrology* 1997; **25**:199–218.
31. Forrer I, Kasteel R, Flury M, Fluhler H. Longitudinal and lateral dispersion in unsaturated field soil. *Water Resource Research* 1999; **35**:3049–3060.
32. Inoue M, Simunek J, Shiozawa S, Hopmans JW. Simultaneous estimation of soil hydraulic and solute transport parameters from transient infiltration experiments. *Advances in Water Resources* 2000; **23**:677–688.
33. Diaw EB, Lehmann F, Ackerer Ph. One-dimensional simulation of solute transfer in saturated-unsaturated porous media using the discontinuous finite elements method. *Journal of Contaminant Hydrology* 2001; **51**:197–213.
34. Ewing RE, Wang H. Eulerian–Lagrangian localized adjoint methods for linear advection equations. *Computational Mechanics'91*. Springer International: Berlin, 1991; 245–250.
35. Wang H, Ewing RE, Celia MA. Eulerian–Lagrangian localized adjoint method for reactive transport with biodegradation. *Numerical Methods in Partial Differential Equations* 1995; **11**:229–254.
36. Celia MA. Eulerian–Lagrangian localized adjoint methods for contaminant transport simulations. In *Computational Methods in Water Resources X*, Peters *et al.* (eds), vol. I. Water Science and Technology Library, vol. 12. Kluwer Academic Publishers: Dordrecht, Netherlands, 1994; 207–216.
37. Wang H, Dahle HK, Ewing RE, Espedal MS, Sharpley RC, Man S. An ELLAM scheme for Advection Diffusion Equations in two dimensions. *SIAM Journal of Scientific Computing* 1999; **20**:2160–2194.
38. Binning P, Celia MA. A forward particle tracking Eulerian–Lagrangian Localized Adjoint Method for solution of the contaminant transport equation in three dimensions. *Advances in Water Resources* 2002; **25**:147–157.
39. Touma J, Vauclin M. Experimental and numerical analysis of two-phase infiltration in a partially saturated soil. *Transport in Porous Media* 1986; **1**:27–55.
40. Celia MA, Bouloutas ET, Zarba RL. A general mass-conservative numerical solution for the unsaturated flow equation. *Water Resources Research* 1990; **26**:1483–1496.
41. Van Genuchten MTh. A closed form equation for predicting the hydraulic conductivity in soils. *Soil Science Society of American Journal* 1980; **44**:892–898.

